Integrating Vector Field Approach and Input-to-State Stability Curved Path Following for Unmanned Aerial Vehicles

Article *in* IEEE Transactions on Systems, Man, and Cybernetics: Systems · June 2018

DOI: 10.1109/TSMC.2018.2839840

CITATIONS
6

READS
288

5 authors, including:

Shulong Zhao
National University of Defense Technology
26 PUBLICATIONS **79** CITATIONS

SEE PROFILE

Xiangke Wang
National University of Defense Technology
94 PUBLICATIONS **780** CITATIONS

SEE PROFILE

Integrating Vector Field Approach and Input-to-State Stability Curved Path Following for Unmanned Aerial Vehicles

Shulong Zhao, Xiangke Wang, Zhiyun Lin, Daibing Zhang, and Lincheng Shen

***Abstract*—In this paper, a curved path following scheme with the aid of the vector field (VF) and the notion of input-to-state stable (ISS) for a fixed-wing unmanned aerial vehicle (UAV) is developed. The VF strategy is a robust and valid guidance method and its stability is proved using ISS properties. Many existing path following algorithms for fixed-wing UAVs are only proposed for straight-lines and orbits. However, the path required to be followed is always in approximate curves rather than straight-lines and orbits in many high-level missions, such as obstacle avoidance, search, and surveillance. The nonlinear-theoretic notion of ISS is playing a central role in the control law design and stability analysis. The error kinematics are converted into two interconnected subsystems with proven ISS properties, which yield the overall system that is globally asymptotically stable, i.e., and the along-track error and the cross-track error asymptotically approach zeros from any initial position in the space. The followed path is defined in terms of the arc-length parameter, and it can be expanded according to the waypoint fitting without the need to obtain a global function representation. The singularity of multiple closest points on the path is eliminated by constructing a speed profile of a virtual point on the path. The scheme is validated with a semi-physical experiment combined by an actual autopilot, ground station and the X-Plane flight simulator. Flight tests using a small fixed-wing UAV show excellent tracking performance of the curved path following.**

***Index Terms*—Curved path following, input-to-state stable (ISS), unmanned aerial vehicles (UAVs), vector field (VF).**

I. Introduction

THERE has been considerable interest over the last few years in the development of miniature unmanned aerial vehicles (UAVs) [1]–[3]. With the rapid improvement of the usefulness of UAVs, the capability of planning and accurately following curved paths are of great importance. Many of the algorithms proposed to settle the guidance and control problem rely on a decomposition procedure, analyzing the requirements of the mission, solving the path planning problem, designing a desired path that conforms to the requirements, and then employing a guide logic to track this desired path [4]. In the majority of actual flight applications, the planned paths are curves, even smooth curves in most cases, rather than straight-lines and orbits (see the surveys [4]–[6]).

Several approaches have been proposed to address the path following problems for small UAVs. In general, as reported in [3], these approaches can be divided in two categories, namely, the geometric methods and the control techniques. The geometric methods, including the pure pursuit [1], line-of-sight (LOS), pure pursuit with LOS (PLOS), nonlinear guidance law [3], L1 method [8] and so on, usually adopt a geometric relation to obtain a virtual target point (VTP), and then forced the UAV to track the VTP [7], [8]. In commercial autopilot systems [9]–[11], the VTP algorithms are the dominating methods for the path following problem due to its easy application, and a crucial issue in those methods is how to update the VTP on the desired path.

The control techniques usually design control commands based on different (nonlinear) control theories to ensure the cross-track error of the UAV converges to zero [12]–[15], [19], [20]. Conversely to the VTP algorithms, the objective is not to follow a ghost vehicle, but to get onto the desired path while moving at a constant airspeed based on the dynamics of the UAVs.

However, it is well known that accurate dynamic models of the miniature UAVs are hard to obtain. Recently, the vector field (VF) method has attracted much attention in path following problems because of its perfect performances and easy implementation (see the survey of [3]). The VF method, belonging to the control techniques, is employed to guarantee that the tracking error of a vehicle asymptotically approaches zero even in the presence of wind disturbances via constructing VFs surrounding the desired path [13].

Then the study is extended to a curved path in [16]. Following this way, Liang *et al.* combines a conservative VF and a solenoidal VF for planar curved path following [17], and a three-dimensional VF that is based on guidance law is proposed for the curved path following problem in [18]. In these methods, an explicit expression of a desired curved path is essential while the explicit expression for a general curved path may be hard to obtain or its expression may be too complex for employing the control law. In addition, in [13]–[15], the cross-track error is defined as the distance to the closest point on the path, which may result in a singularity when the number of closest points exceeds one, i.e., the

Manuscript received December 25, 2017; accepted May 9, 2018. This paper was recommended by Associate Editor X. Xu. *(Corresponding author: Shulong Zhao.)*

S. Zhao, X. Wang, D. Zhang, and L. Shen are with the College of Mechanics and Automation, National University of Defense Technology, Changsha 410073, China (e-mail: jaymaths@nudt.edu.cn).

Z. Lin is with the College of Electrical Engineering, Zhejiang University, Hangzhou 310027, China.

Color versions of one or more of the figures in this paper are available online at http://ieeexplore.ieee.org.

Digital Object Identifier 10.1109/TSMC.2018.2839840

UAV is positioned at the center of curvature for a point on the path.

It is worth pointing out that the curved path following methods have not received extensive attention and implementation in autopilot controllers. For example, the work done in [7] and [12]–[15], is only developed for straight lines and orbits path following.

To our best knowledge, all existing autopilots including the Pixhawk [9], Paparazzi [10] and so on, are not equipped with the function of curved path following. Instead, only paths in straight-lines or orbits (or combinations of lines and orbits) are considered. The biggest obstacle to the straight path following method that cannot be extended directly to a curved path is that the heading of the desired point on the path could not be considered.

The study presented in this paper focuses on the curved path following problem for miniature UAVs flying in two dimensions at a constant speed with the aid of the input-to-state stable (ISS) notion. The ISS concept describes how external inputs affect the internal stability of nonlinear systems (see [21] for a tutorial). In the proposed method, instead of projecting the UAV position onto the path, the control law designs a self-adaptive speed parameter to drive a VTP to propagate on the path, and the path error is defined as the distance between the UAV and the VTP. The solution has a sufficient real-world scenario and can be directly applied to flight experiments with minor adjustments. To verify the effectiveness of the proposed path following algorithm, different gain parameters are considered in experiments and the one with the best performance is selected.

To our knowledge, while VF guidance method has been reported for the small fixed-wing UAV applications [3], [5], [13], [16]–[18], approaches for the VF control guidance scheme integrated with the ISS for the small fixed-wing UAV curved path following have not been seen in open literature to date. Unlike the VF method in [13], the path to be followed here can be straight lines, orbits, B-splines or any other smooth and differentiable curves. Unlike some existing curved path following approaches, such as the study in [20], the path to be followed is defined in terms of the arc-length parameter in Frenet–Serret frame [24], rather than in Cartesian space with (x, y) descriptors. Unlike work in [31], we especially take the curvature of the followed path into account and the tracking performance will be better when the curvature of the desired path is rapidly altered.

Compared with the results in [10]–[17], the proposed scheme in this paper has the following contributions.

1) We construct a VF approach for the curved path following for a fixed-wing UAV. The singularity of multiple closest points on the path is eliminated by constructing a speed profile for a VTP on the path. In other words, we have solved the geometric task with speed assignment of a maneuvering problem defined in [23].
2) The nonlinear-theoretic notion of ISS is playing a central role in the control law design and stability analysis. In the proposed scheme, the error kinematics are transformed into a two-cascade interconnected system with proven ISS properties, resulting in global asymptotic stability of the overall system, i.e., the along-track error and cross-track error approach zeros asymptotically from any initial position.
3) The desired path is produced using a B-spline to pass through the predefined waypoints that could be expanded with new added waypoints without the need to obtain a global function representation.
4) We explicitly consider the curvature of the desired path in the designation of guidance logic, which eliminates any issues related to the combination of different VFs of path segments with the curvature set to 0 (straight line) or $1/R$ (circle).

II. Preliminaries and Problem

A. Input-to-State Stable

A function $\gamma : \mathbb{R}_+ \to \mathbb{R}_+$ is of *class* $\mathcal{K}$ if it is continuous, strictly increasing and $\gamma(0) = 0$; it is of *class* $\mathcal{K}_\infty$ if it is unbounded. In addition, a function $\beta : \mathbb{R}_+ \times \mathbb{R}_+ \to \mathbb{R}_+$ is of class $\mathcal{KL}$; it is of *class* $\mathcal{K}$ in the first part and strictly decreasing to zero in the second part.

Consider the nonlinear system with $w \in \mathbb{R}^m$ as the external input and $x \in \mathbb{R}^n$ as the state, and we have

$$\dot{x}(t) = f(x(t), w(t)) \tag{1}$$

where $f : \mathbb{R}^n \times \mathbb{R}^m \to \mathbb{R}^n$ is a locally Lipschitz function.

Definition 1 [21]: The system (1) is said to be ISS with w used as input if there exists a class $\mathcal{KL}$ function β and a class $\mathcal{K}$ function γ such that, for each initial condition $x(0)$ and each measurable essentially bounded input $w(\cdot)$ defined on $[0, \infty)$, the solution $x(\cdot)$ exists on $[0, \infty)$ and satisfies

$$|x(t)| \le \beta(|x(0)|, \gamma(\|w\|)) \quad \forall t \ge 0. \tag{2}$$

Not surprisingly, if the system $\dot{x} = f(x, w)$ with w used as the input in (1) is ISS, then the unforced system $\dot{x} = f(x, 0)$ is globally asymptotically stable (GAS) at $x = 0$ [21].

Definition 2 [21]: Consider a nonlinear system (1). A function V is regarded as an *ISS-Lyapunov function* if it is differentiable almost everywhere, and satisfies the following.

1) V is positive definite and radially unbounded, that is, there exist $\underline{\alpha}, \overline{\alpha} \in \mathcal{K}_\infty$ such that

$$\underline{\alpha}(|x|) \le V(x) \le \overline{\alpha}(|x|) \quad \forall x \in \mathbb{R}^n. \tag{3}$$

2) There exists a positive definite function α, and a class $\mathcal{K}$ function γ such that

$$\dot{V}(x, u) \le -\alpha(V(x)) + \gamma(|w|) \quad \forall x \in \mathbb{R}^n \ \forall w \in \mathbb{R}^m. \tag{4}$$

Lemma 1 [21]: The system (1) is ISS if and only if it admits a smooth ISS-Lyapunov function.

Lemma 2 [21], [22]: Consider a cascade system

$$\dot{z} = f(z, x) \tag{5}$$

$$\dot{x} = g(x, u). \tag{6}$$

If each of the two subsystems is ISS, i.e., each subsystem admits an ISS-Lyapunov function, then the cascade system is also ISS. Further, a special case in which the x-subsystem has no inputs, the cascaded system of one GAS and one ISS is GAS.

B. Problem Formulation

In many typical missions of UAVs, the airspeed and the altitude are kept constant [1], [3], [5]. That is to say, the autopilot of a UAV has an independent airspeed controller and an altitude controller that hold the airspeed and altitude constant. Therefore, this paper considers the curved path following problem of a fixed-wing UAV with the assumption that the altitude and airspeed controllers are well adjusted to hold constant (or nearly constant) altitude and airspeed, respectively. Immediately, a planar model in inertial coordination is employed to perform a coordinated flight shown in (7). It is worth pointing out that the model is widely used in the field of path following of fixed-wing UAVs, and suitable for describing the navigational dynamics of most common distributed fixed-wing UAVs [3], [13], [14]

$$\begin{cases} \dot{x} = V_g \cos\chi \\ \dot{y} = V_g \sin\chi \\ \dot{\chi} = \omega \end{cases} \tag{7}$$

where (x, y) and χ denote the inertial position and the course of the UAV. V_g and ω represent the groundspeed and the angular speed (yaw rate) of the UAV, respectively.

Remark 1: Note that navigational dynamics (7) are presented in terms of the course angle χ and groundspeed V_g, which are independent of the wind. It is reported in [13] that wind-disturbance rejection can be improved significantly by using ground-referenced measurements (i.e., χ and V_g), compared with the model represented by the heading angle(ψ) and airspeed (V_a).

The inertial position of the UAV is $p = [x, y]^T \in \mathbb{R}^2$. According to (7), it is obtained that

$$\dot{p} = \left[\dot{x}, \dot{y}\right]^T = \left[V_g \cos\chi, V_g \sin\chi\right]^T = R(\chi)\begin{bmatrix} V_g \\ 0 \end{bmatrix} \tag{8}$$

where

$$R(\chi) = \begin{bmatrix} \cos\chi & -\sin\chi \\ \sin\chi & \cos\chi \end{bmatrix}. \tag{9}$$

Formally, the path following problem can be defined in the Frenet–Serret frame [24]. The geometric path is defined in terms of some arc-length parameters, provided that it is differentiable. For any given arc-length s relative T_0, a starting point on the path, the inertial position of the point on the path associated with s is denoted by $q(s) = [x_q(s), y_q(s)] \in \mathbb{R}^2$. The Frenet–Serret frame is attached and a VTP moves along the path at speed $\dot{s}$. The x-axis of the Frenet–Serret frame is aligned with the tangent vector to the path at $q(s)$ and has an angle $\chi_f(s)$ with respect to the inertial frame. It is clear that

$$\dot{q} = [\dot{x}_q(s), \dot{y}_q(s)]^T = R(\chi_f)\begin{bmatrix} \dot{s} \\ 0 \end{bmatrix} \tag{10}$$

where

$$R(\chi_f) = \begin{bmatrix} \cos\chi_f & -\sin\chi_f \\ \sin\chi_f & \cos\chi_f \end{bmatrix} \tag{11}$$

is the rotation matrix from the Frenet–Serret frame to the inertial frame.

Let the error vector e in the Frenet–Serret frame be decomposed into the along-track error e_s and the cross-track error e_d. Then the inertial error vector is obtained by

$$e = [e_s, e_d]^T = R^T(\chi_f)(p - q(s)). \tag{12}$$

By differentiating (12) with respect to time, it follows that:

$$\dot{e} = \dot{R}^T(\chi_f)(p - q(s)) + R^T(\chi_f)(\dot{p} - \dot{q}(s)). \tag{13}$$

Note that for a rotational matrix $R(\chi_f) \in SO(2)$ (the special orthogonal group in dimension 2), it is obvious that [25]

$$\dot{R}(\chi_f) = R(\chi_f)S\left(\dot{\chi}_f\right) \tag{14}$$

with

$$S\left(\dot{\chi}_f\right) = \begin{bmatrix} 0 & -\dot{\chi}_f \\ \dot{\chi}_f & 0 \end{bmatrix}. \tag{15}$$

Note that $S(\dot{\chi}_f) = -S^T(\dot{\chi}_f)$ is a skew-symmetric matrix.

Considering (8), (10), and (14), (13) is rewritten by

$$\begin{aligned} \dot{e} = {} & S^T\left(\dot{\chi}_f\right)R^T\left(\chi_f\right)(p - q(s)) \\ & + R^T\left(\chi_f\right)\left(R(\chi)\begin{bmatrix} V_g \\ 0 \end{bmatrix} - R\left(\chi_f\right)\begin{bmatrix} \dot{s} \\ 0 \end{bmatrix}\right). \end{aligned}$$

Together with $R^T(\chi_f)R(\chi) = R(\chi - \chi_f)$, it follows that:

$$\dot{e} = -S\left(\dot{\chi}_f\right)e + R\left(\chi - \chi_f\right)\begin{bmatrix} V_g \\ 0 \end{bmatrix} - \begin{bmatrix} \dot{s} \\ 0 \end{bmatrix}. \tag{16}$$

Further, the error course angle $\tilde{\chi}$ denotes as $\tilde{\chi} \triangleq \chi - \chi_f$. Hence, we obtain the time derivative of $\tilde{\chi}$

$$\dot{\tilde{\chi}} = \dot{\chi} - \dot{\chi}_f = \omega - \kappa(s)\dot{s}$$

because of $\dot{\chi}_f = (d\chi_f/dt) = (d\chi_f/ds)(ds/dt) = \kappa(s)\dot{s}$, where $\kappa(s)$ is the curvature of the path at $q(s)$ with respect to s.

Therefore, the error kinematic model of a fixed-wing UAV for the curved path following problem with respect to the Frenet–Serret frame is:

$$\begin{aligned} \dot{e}_s &= V_g \cos\tilde{\chi} - (1 - \kappa(s)e_d)\dot{s} \\ \dot{e}_d &= V_g \sin\tilde{\chi} - \kappa(s)e_s\dot{s} \\ \dot{\tilde{\chi}} &= \omega - \kappa(s)\dot{s}. \end{aligned} \tag{17}$$

For the kinematics (17), our control objective is to design proper control inputs (ω and $\dot{s}$), such that e_s and e_d approach zeros.

III. Main Results

A. Error Kinematic Model Based on VF

According to the kinematics (17), a differentiable VF $\chi_d(e_d) \in (-\chi^\infty, \chi^\infty)$ is constructed, where $\chi^\infty \in (0, \pi/2]$, and $-\chi_d(e_d)$ is a class $\mathcal{K}$ function and globally Lipschitz, with respect to the cross-track error e_d satisfying

$$\underline{k}_{\chi_d}|e_d| \le |-\chi_d(e_d)| \le \bar{k}_{\chi_d}|e_d| \quad \forall \ e_d \tag{18}$$

where $\bar{k}_{\chi_d} > \underline{k}_{\chi_d} > 0$ are Lipschitz constants.

A possible VF, for example, can be depicted as follows [30]:

$$\chi_d(e_d) = -\chi^\infty \frac{e^{2ke_d} - 1}{e^{2ke_d} + 1} \tag{19}$$

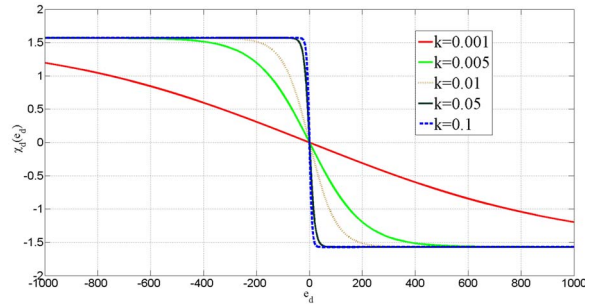

Fig. 1. Illustration of $\chi_d(e_d)$ depicted by (19) with respect to e_d.

where $\chi^\infty \in (0, \pi/2]$ is a constant angle, and $k > 0$ is a control parameter, which controls the rate of convergence of e_d. The angle $\chi_d(e_d)$ is directed toward 0 when the absolute value of e_d is small and approaches $-\chi^\infty$ when $|e_d|$ is large.

And further, we have

$$4k\chi^\infty \frac{e^{2ke_d^m}}{\left(e^{2ke_d^m}+1\right)^2}|e_d| \le |-\chi_d(e_d)| \le k\chi^\infty |e_d|.$$

where e_d^m is the bound of e_d, i.e., $|e_d| \le e_d^m$. The evolutions of $\chi_d(e_d)$ in (19) with different parameters k are illustrated in Fig. 1.

It is noted that

$$e_d \sin(\chi_d(e_d)) \le 0 \quad \forall \quad e_d \tag{20}$$

as e_d and $\chi_d(e_d)$ are found with different signs exactly, and the $\sin(\cdot)$ function is strictly increasing in $(-\pi/2, \pi/2)$.

The desired course of the UAV is specified by the direction of the VFs, namely, the error course angle $\tilde{\chi}$ is required to approach the VFs. Therefore, when the cross-track error e_d is large, the UAV is directed to approach the path with error course χ^∞ that, as e_d approaches zero, the course angle tends to the direction of the path.

In the following, symbol χ_d is used to represent $\chi_d(e_d)$ for short. The mismatch between the error course angle $\tilde{\chi}$ and its corresponding VF χ_d is defined by

$$e_\chi = \tilde{\chi} - \chi_d. \tag{21}$$

Correspondingly, we have $\tilde{\chi} = e_\chi + \chi_d$, and the error kinematic model in (17) can be rewritten as

$$\dot{e}_s = V_g \cos(e_\chi + \chi_d) - (1 - \kappa(s)e_d)\dot{s} \tag{22}$$

$$\dot{e}_d = V_g \sin\left(e_\chi + \chi_d\right) - \kappa(s)e_s\dot{s} \tag{23}$$

$$\dot{e}_\chi = \omega - \kappa(s)\dot{s} - \dot{\chi}_d. \tag{24}$$

B. Path Following Law Design

Looking at (22)–(24). They can be treated as a cascade system of two subsystems. For (24), the input is ω and the state is e_χ; whereas for (22) and (23), the input is e_χ and states are $[e_s, e_d]$. In the sequel, two lemmas are provided regarding the two subsystems.

Lemma 3: The system (22) and (23), with

$$\dot{s} = k_s e_s + V_g \cos\tilde{\chi} \tag{25}$$

where $k_s > 0$ is a positive constant, with e_χ and $[e_s, e_d]$ representing the input and states, respectively, is an ISS.

Proof: For system (22) and (23), a Lyapunov function candidate

$$W_1(e_d, e_s) = \frac{1}{2}\left(e_s^2 + e_d^2\right)$$

is employed. Clearly, it is easy to find two classes of $\mathcal{K}$ functions $k_1(e_s, e_d)$ and $k_2(e_s, e_d)$, satisfies

$$k_1(e_s, e_d) \le W_1(e_d, e_s) \le k_2(e_s, e_d) \quad \forall \quad e_s, e_d.$$

Differentiating both sides of W_1, it is obtained that

$$\dot{W}_1(e_d, e_s) = e_d\dot{e}_d + e_s\dot{e}_s.$$

By using (17), we obtain

$$\begin{aligned}\dot{W}_1 &= e_d\left(V_g \sin\tilde{\chi} - \kappa(s)e_s\dot{s}\right) + e_s\left(V_g\cos\tilde{\chi} - (1-\kappa(s)e_d)\dot{s}\right)\\ &= e_d V_g \sin\tilde{\chi} + e_s V_g \cos\tilde{\chi} - e_s\dot{s}.\end{aligned}$$

Considering (25), we have

$$\begin{aligned}\dot{W}_1 &= e_d V_g \sin\tilde{\chi} - k_s e_s^2\\ &= V_g e_d \sin\chi_d - k_s e_s^2 + V_g e_d(\sin\tilde{\chi} - \sin\chi_d).\end{aligned} \tag{26}$$

Further, as $\chi_d \in (-\pi/2, \pi/2)$, it is known that $\sin(\chi_d)$ is monotone increasing with respect to χ_d, therefore we have $(2/\pi)|\chi_d| \le |\sin\chi_d| \le |\chi_d|$. Moreover, if and only if $\chi_d = 0$, then the equivalence is achieved. Therefore,

$$\frac{2}{\pi}|e_d||\chi_d| \le |e_d \sin\chi_d| \le |e_d||\chi_d|.$$

As $e_d\sin\chi_d$ and $e_d\chi_d$ are both always less than zero, we have

$$e_d\chi_d \le e_d\sin\chi_d \le \frac{2}{\pi}\chi_d e_d \le 0.$$

Considering χ_d is globally Lipschitz, (18), yields

$$-\bar{k}_{\chi_d}e_d^2 \le e_d\sin\chi_d \le -\frac{2\underline{k}_{\chi_d}}{\pi}e_d^2 \le 0. \tag{27}$$

Note that

$$\begin{aligned}|\sin\tilde{\chi} - \sin\chi_d| &= \left|\sin\left(e_\chi + \chi_d\right) - \sin\chi_d\right|\\ &= \left|\sin e_\chi\cos\chi_d + \cos e_\chi\sin\chi_d - \sin\chi_d\right|\\ &= \left|\sin e_\chi\cos\chi_d + \left(\cos e_\chi - 1\right)\sin\chi_d\right|\\ &\le \left|\sin e_\chi\cos\chi_d\right| + \left|\left(\cos e_\chi - 1\right)\sin\chi_d\right|\\ &\le 2|e_\chi|.\end{aligned}$$

Therefore, considering $|e_d|$ is bounded in practice, there always exists a class of $\mathcal{K}$ function $\gamma_\chi(|\cdot|)$

$$\left|V_g e_d(\sin\tilde{\chi} - \sin\chi_d)\right| \le 2V_g|e_d||e_\chi| \le \gamma_\chi\left(|e_\chi|\right). \tag{28}$$

With the aid of (27) and (28), $\dot{W}_1$ in (26) yields

$$\begin{aligned}\dot{W}_1 &\le -V_g\frac{2\underline{k}_{\chi_d}}{\pi}e_d^2 - k_s e_s^2 + \gamma_\chi\left(|e_\chi|\right)\\ &\le -2\min\left(\frac{2V_g\underline{k}_{\chi_d}}{\pi}, k_s\right)W_1(e_d, e_s) + \gamma_\chi\left(|e_\chi|\right).\end{aligned}$$

Therefore, according to Lemma 1, the ISS of the system is concluded. ■

Lemma 4: The state e_χ in system (24) will globally exponentially converges to zero with control laws

$$\omega = -k_\omega(\tilde{\chi} - \chi_d) + \kappa(s)\dot{s} + \dot{\chi}_d \tag{29}$$

where k_ω is positive.

Proof: Consider a Lyapunov function candidate

$$W_2(e_\chi) = \frac{1}{2}e_\chi^2.$$

If and only if $e_\chi = 0$, i.e., $\tilde{\chi} = \chi_d$, then the equivalence is achieved.

By differentiating both sides of W_2 with respect of time, and then considering (24), it is obtained that

$$\dot{W}_2(e_\chi) = e_\chi \dot{e}_\chi = e_\chi(\omega - \kappa(s)\dot{s} - \dot{\chi}_d).$$

With the aid of (29), it is obtained that

$$\dot{W}_2(e_\chi) = -k_\omega e_\chi^2 = -2k_\omega W_2(e_\chi)$$

which finishes the proof. ■

Now, it is time to present our main result.

Theorem 1: The system of kinematics (17), with control laws (25) and (29), is globally asymptotically stable. That is, the errors $[e_s, e_d]$ converge to zeros asymptotically, and $\tilde{\chi}$ converges to χ_d.

Proof: It is known that kinematics (17), with control laws (25) and (29), can be taken as a cascade system of two subsystems. From Lemma 4, it is known that, the e_χ-subsystem, composed of (17) and (29), is clearly GAS, as e_χ is globally exponentially converges to zero. And from Lemma 3, taking e_s and e_d as the states and e_χ as the input, the system described by (22) and (23), as $\dot{s}$ is designed by (25), is ISS. Therefore, according to Lemma 2, the overall system, consisting of (17), (25), and (29), is also GAS. Thus, the errors $[e_s, e_d]$ converge to zeros asymptotically, and $\tilde{\chi}$ converges to χ_d. ■

C. Algorithm Realization

Based on the theoretical foundation in the previous description, the curved path following algorithm in Theorem 1, when the VF is using (19), is realized as Algorithm 1.

In Algorithm 1, the function *curvefun(s)* is monotonic with respect to the arc-length s. It is used to describe the characters of the reference path, and return the position $q(s)$, the angle $\chi_f(s)$, and the curvature $\kappa(s)$, with respect to the parameter s.

It is worth pointing out that the function *curvefun(s)* can be any type of curve, provided that it is differentiable. In order to enhance practicality, all the desired paths we use are generated by waypoints matching, so we need a smooth path between the waypoints. At the same time, in order to maintain the continuity of curvature, we need the desired path to meet the differentiable conditions.

Remark 2: When this algorithm is implemented in the autopilot, the update frequency is 200 Hz. In each control cycle, the distance between the two update points is very close. It can be almost considered that the curved path is obtained by splicing many linear segments with very small curvature. Therefore, there is no phenomenon that the vehicle takes a shortcutİ when tracking a curved path.

Algorithm 1 VF-Based Curved Path Following

1: Initialize: k_s, k_ω, and k;
2: Obtain the state of UAV: $[p, \ \chi]$;
3: Obtain the descriptors of curved path by function $[q(s), \chi_f, \kappa(s)] = curvefun(s)$;
4: $\tilde{\chi} = \chi - \chi_f$;
5: Compute along-track and cross-track errors by using

$$\begin{bmatrix} e_s \\ e_d \end{bmatrix} = \begin{bmatrix} \cos\chi_f & \sin\chi_f \\ -\sin\chi_f & \cos\chi_f \end{bmatrix}(p - q);$$

6: $\dot{s} = k_s e_s + V_g \cos\tilde{\chi}$;
7: Set $\chi^\infty = \pi/2$;
8: $\chi_d = -\chi^\infty \frac{e^{2ke_d}-1}{e^{2ke_d}+1}$;
9: $\nabla\chi_d = -4k\chi^\infty \frac{e^{2ke_d}}{(e^{2ke_d}+1)^2}$;
10: $e_\chi = \tilde{\chi} - \chi_d$, and then limit e_χ into $(-\pi, \pi]$;
11: $\omega = -k_\omega e_\chi + \kappa\dot{s} + \nabla\chi_d(V_g \sin\tilde{\chi} - \kappa e_s\dot{s})$.

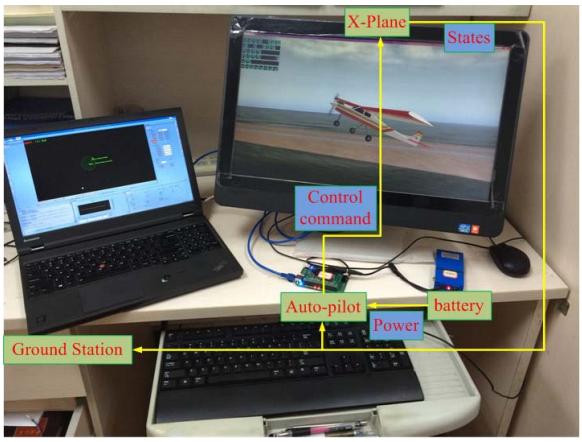

Fig. 2. High-fidelity semi-physical experiment environment, constructed by an actual autopilot, a ground station and the X-plane flight simulator.

IV. Experiments

A. Simulation

To verify the effectiveness and applicability of the proposed control strategy, we developed a high-fidelity semi-physical experiment scheme. The proposed approach has been simulated in an X-plane environment [26], which provides very accurate aircraft models and has the possibility of exchanging data with external systems. The aircraft models simulated in the X-plane are based on the exact physical model and material.

The entire system consists of three segments, namely the ground control station, autopilot, and X-plane as shown in Fig. 2 [27]. We employ the X-plane to provide the exact physical model and material of the UAV in the experiments; the X-plane can be used to establish the flight environment conditions. The conditions of the flight environment can be established. The majority of the conditions are independent of this paper, and the wind and turbulence are established in the low-altitude layer (below 2000 feet).

The *Great Planes PT-60 RC plane* is employed in the experiments as shown in Fig. 3. The frame of the plane and its

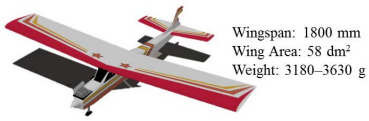

Fig. 3. Great planes PT-60 RC plane, and its main parameters in the X-plane flight simulator.

main parameters are: Wingspan, 1800 mm, Wing area, 58 dm^2, Weight, 3180 g.

The aircraft has a traditional configuration, and the desired curved path is generated by cube spline interpolation. Consider eight waypoints in Table I, where Lon and Lat represent the longitude and the latitude, respectively.

1) Predefined Path: Based on the distance, orientation, and curvature, smooth curvature profiles can be easily provided. In particular, double continuous curvature paths, which consist of a combination of clothoids, line segments and arcs, are extensively employed. Some practical applications, such as obstacle avoidance, differ from cruising or investigation because the change in curvature and orientation is acute and unexpected.

A B-spline curve $S : [0, 1] \rightarrow R^2$ is defined as

$$S(u) = \sum_{i=0}^{m} P_i N_{i,p}(u) \tag{30}$$

where, P_i is the control point. $N_{i,p}(u)$ is defined by the Cox-de Boor iterative formula

$$N_{i,0}(u) = \begin{cases} 1, & \text{if } u_i \le u \le u_{i+1} \\ 0, & \text{otherwise} \end{cases}$$
$$Ni, p(u) = \frac{u - u_i}{u_{i+p} - u_i} N_{i,p-1}(u) + \frac{u_{i+p+1} - u}{u_{i+p+1} - u_{i+1}} N_{i+1,p-1}(u) \tag{31}$$

where u_i denotes knots, and $u_0 \le u_1 \le \ldots \le u_m$. The number of knots is $m + 1$, $U = [u_0, u_1, \ldots, u_m]$ is a knot vector, and p is the degree of the basic function. We define $p = 3$ in our simulations.

2) Resluts: The parameters in Algorithm 1 are as follows: $k_s = 1$, $k_p = 1$, $\lambda = 1$, $\underline{k}_{\chi_d} = 0.1$, $\xi = \pi^2/4$, and $\epsilon = 5 * 180/\pi$. The velocity of the UAV is 15 m/s, and the wind speed ranges from 3 to 7 m/s from 90° southwest, which indicates that the wind speed accounts for 20%–50% of the airspeed of the UAV.

To perform curved path following, the pitch of the UAV is needed to maintain a given altitude (100 m in this paper), and the yaw is the major controlled angle in the process of path following. However, the change in heading is related to the roll.

To obtain a proper description of the tracking error in a curved path, a minimum distance to the arc must be defined. We consider the points in the flown path form a center, and find a circle with a small radius. The desired path is on the boundary of the circle. We also implement the combined VF method proposed in [17], adaptive backstepping method proposed in [29] and integral LOS method proposed in [30] to compare the tracking performances.

The VFs in [17] are defined as

$$\mathbf{v}_d = -\tanh(\kappa r)\mathbf{v}_c + s\,\mathrm{sec}(\kappa r)\mathbf{v}_s \tag{32}$$

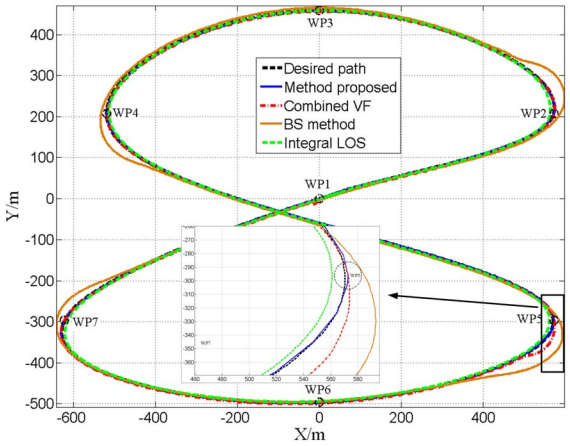

Fig. 4. Tracking results of the UAV with different methods.

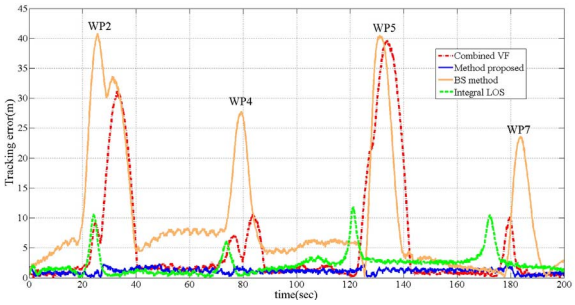

Fig. 5. Tracking error of the UAV.

where, $\mathbf{v}_c$ is a conservative VF, and $\mathbf{v}_s$ is a solenoidal VF. The scaling factor κ is chosen equal to 0.3.

The tracking results and tracking error of the four methods are shown in Figs. 4 and 5, respectively. When the curvature of the desired path is slowly altered, and the tracking error of our method, the combined VF and Integral LOS method are similar. Conversely, if the curvature of the desired path is rapidly altered (nearby WP2, WP4, WP5, and WP7), and the tracking error of the combined VF and integral LOS are much larger than that of our method. Our method has a better tracking performance for a general curved path.

To test the robustness and capabilities of the proposed path following algorithms, many other types of parameters have been tested. In our method, the most important parameters are k_s, k_p, and k. The gain parameters are

$$\begin{aligned} k_s &\in (0.1, 0.5, 1, 1.5) \\ k_p &\in (0.1, 0.5, 1, 1.5) \\ k &\in (0.005, 0.01, 0.05). \end{aligned} \tag{33}$$

For a given group of parameters, we define $u(t)$ and $e(t)$ as the control input and tracking error at time t. The total control inputs and tracking errors are defined as

$$\begin{aligned} \Sigma|U|^2 &= \sum_{t=0}^{t=T} u(t)^2 \\ \Sigma|D|^2 &= \sum_{t=0}^{t=T} e(t)^2. \end{aligned} \tag{34}$$

TABLE I
POSITIONS OF WAYPOINTS

Waypoint	WP1	WP2	WP3	WP4	WP5	WP6	WP7	WP8
Lon/deg	124.296	124.29319	124.2898	124.29319	124.3	124.3027	124.3	124.296
Lat/deg	48.2661	48.27125	48.2661	48.26143	48.27125	48.2661	48.2605	48.2661
x/m	0	572.65	0	-519.28	572.65	0	-622.7	0
y/m	0	207.99	458.92	207.99	-296.07	-495.93	-296.08	0

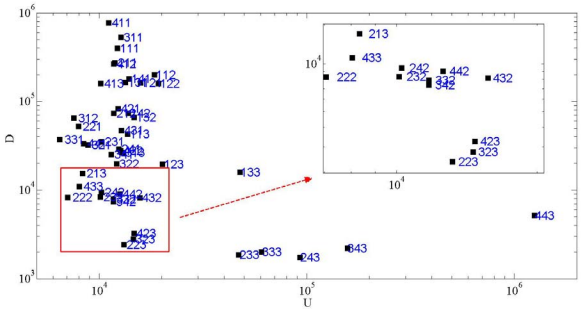

Fig. 6. Parameters of the proposed path-following algorithm for different gain parameters.

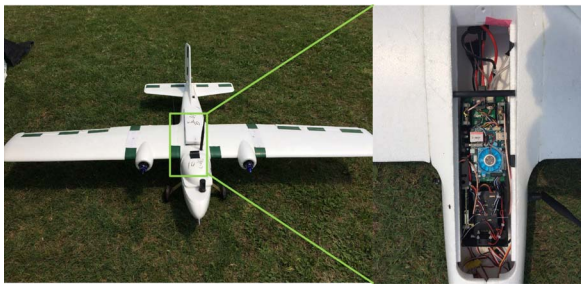

Fig. 7. Small fixed-wing UAV used in flight tests.

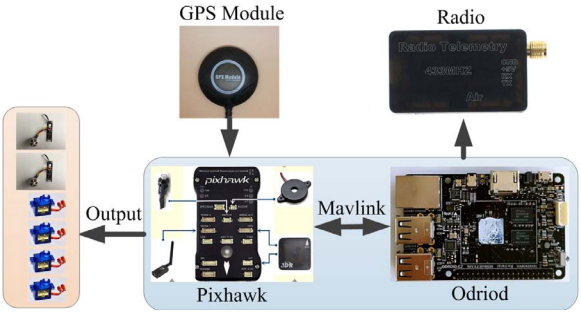

Fig. 8. Test apparatu combined with two segments: Odroid-XU4 computer and Pixhawk autopilot.

The performance of the method is dependent on the values of the gain parameters. To present the performance of the proposed control strategy with different parameters, we plot the relation between the total control input and the tracking error of each group of parameters. The gain parameters k_s, k_ω, and k are selected from the sets $k_s \in (0.1, 0.5, 1, 1.5)$, $k_p \in (0.1, 0.5, 1, 1.5)$, and $k \in (0.005, 0.01, 0.05)$, respectively.

For example, 221 refers to $k_s(2) = 0.5$, $k_p(2) = 0.5$, and $k(1) = 0.005$. The effects of the different control parameters on the system response are tested by increasing one parameter through four values from the minimum to the maximum value while holding the other parameters constant.

As shown in Fig. 6, the parameters 223, $k_s = 1.5, k_p = 1.5, k = 0.05$, are the best gain parameters. Although the initial position of the UAV is close to the path, the convergence is very slow when k is very small. If we choose a large k, the path following convergence accelerates and causes a flattering trajectory due to practical constants of control. A similar phenomenon exists for k_p.

B. Flight Test

The curved path following algorithm is implemented and validated with a real fixed-wing UAV. As shown in Fig. 7, the wing span of the vehicle is 1800 mm and the body length is 1220 mm. The total weight of the vehicle is 1.1 kg and maximum take-off weight is 4.6 kg. Fig. 8 shows the test apparatu combined with two segments: 1) Odroid-XU4 computer and 2) Pixhawk autopilot. We implement Algorithm 1 proposed in this paper with Odroid-XU4, which is a new computing device with more powerful, more energy-efficient hardware based on Ubuntu 14.04. The Pixhawk autopilot is employed to act as the control loop, which controls the vehicle to follow the desired velocity, desired altitude, and desired heading angle obtained from the output of Odroid. The mavlink protocol is used to connect the host computer (Odroid) and the autopilot. The parameters of Pixhawk autopilot could be readjusted well after several flight tests. Two different algorithms, VF and PLOS, are tested and compared. For the PLOS algorithm, the desired heading angle rate is obtained [3]

$$\omega = k_e \tilde{\chi} + k_d e_d. \tag{35}$$

The parameters of the algorithm VF are selected as $k_s = 1.5, k_p = 1.5, k = 0.05$, and parameters of the algorithm PLOS are employed as $k_e = 1.2, k_d = 0.05$. For fair comparison, we implement two algorithms with the same desired path, which is interpreted by (30) and (31) with 22 waypoints.

The curved path following results are shown in Fig. 9, while the tracking error is given in Fig. 10. As shown in the figure, both algorithms exhibit good path following performance despite the wind disturbance is 6–8 m/s, and the velocity of the UAV is 17 m/s. The plot shows the trajectories of the UAV (red and green lines) on a desired path (blue dotted line) passing all waypoints. Fig. 10 shows the tracking error of the vehicle during the whole following phase. The mean following errors on the curved path are 6.72 and 15.23 m for the VF method and the PLOS method, respectively. The results show that the vehicle using the VF method moves along the desired path better than using the PLOS method.

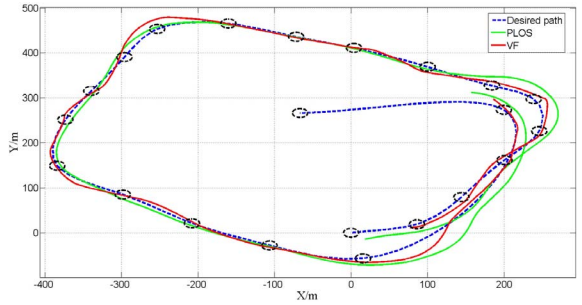

Fig. 9. Tracking results of two different algorithms.

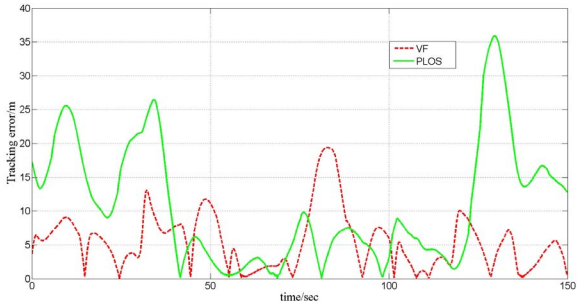

Fig. 10. Tracking errors of two different algorithms.

V. Conclusion

In this paper, a new curved path following method for UAVs based on the VFs has been proposed. Using concepts of the cascaded ISS systems, the stability of the path following algorithm is concluded. The singularity of multiple closest points on the path is eliminated by constructing a speed profile of a virtual point on the path. The method can be extended to include multiple UAVs, allowing the scheme to be used for formation path following control. The effectiveness of the proposed algorithm has been demonstrated in high-fidelity semi-physical simulations with *Auto-Pilot* and *X-Plane* flight simulator in-loop. Meanwhile, the curved path following algorithm is also implemented and validated with a real fixed-wing UAV in flight tests. Further, wind disturbances will be considered to ensure the robustness to wind, and flight experiments in a fixed-wing UAV are employed on the way. More comparisons with different path following algorithms are also considered.

References

[1] B. Xu, "Composite learning finite-time control with application to quadrotors," *IEEE Trans. Syst., Man, Cybern., Syst.*, to be published.
[2] B. Xu, "Disturbance observer-based dynamic surface control of transport aircraft with continuous heavy cargo airdrop," *IEEE Trans. Syst., Man, Cybern., Syst.*, vol. 47, no. 1, pp. 161–170, Jan. 2017.
[3] P. B. Sujit, S. Saripalli, and J. B. Sousa, "Unmanned aerial vehicle path following: A survey and analysis of algorithms for fixed-wing unmanned aerial vehicless," *IEEE Control Syst.*, vol. 34, no. 1, pp. 42–59, Feb. 2014.
[4] S. LaValle, *Planning Algorithms*. Cambridge, U.K.: Cambridge Univ. Press, 2006, pp. 25–40.
[5] C. Goerzen, Z. Kong, and B. Mettler, "A survey of motion planning algorithms from the perspective of autonomous UAV guidance," *J. Intell. Robot Syst.*, vol. 57, no. 1, pp. 65–100, 2010.
[6] N. Dadkhah and B. Mettler, "Survey of motion planning literature in the presence of uncertainty: Considerations for UAV guidance," *J. Intell. Robot. Syst.*, vol. 65, nos. 1–4, pp. 233–246, 2012.
[7] G. Ambrosino *et al.*, "Path generation and tracking in 3-D for UAVs," *IEEE Trans. Control Syst. Technol.*, vol. 17, no. 4, pp. 980–988, Jul. 2009.
[8] S. Park, J. Deyst, and J. P. How, "Performance and Lyapunov stability of a nonlinear path following guidance method," *J. Guid. Control Dyn.*, vol. 30, no. 6, pp. 1718–1728, 2007.
[9] (2015). *Pixhawk Autopilot*. [Online]. Available: https://pixhawk.org/modules/pixhawk
[10] (2015). *Pixhawk Autopilot*. [Online]. Available: http://paparazzi.enac.fr
[11] (2015). *Pixhawk Autopilot*. [Online]. Available: http://www.cloudcaptech.com
[12] P. Coelho and U. Nunes, "Path-following control of mobile robots in presence of uncertainties," *IEEE Trans. Robot.*, vol. 21, no. 2, pp. 252–261, Apr. 2005.
[13] D. R. Nelson, D. B. Barber, T. W. McLain, and R. W. Beard, "Vector field path following for miniature air vehicles," *IEEE Trans. Robot.*, vol. 23, no. 3, pp. 519–529, Jun. 2007.
[14] R. W. Beard, J. Ferrin, and J. Humpherys, "Fixed wing UAV path following in wind with input constraints," *IEEE Trans. Control Syst. Technol.*, vol. 22, no. 6, pp. 2103–2117, Nov. 2014.
[15] A. P. Aguiar and J. P. Hespanha, "Trajectory-tracking and path-following of underactuated autonomous vehicles with parametric modeling uncertainty," *IEEE Trans. Autom. Control*, vol. 52, no. 8, pp. 1362–1379, Aug. 2007.
[16] S. Griffiths, "Vector field approach for curved path following for miniature aerial vehicles," in *Proc. AIAA Guid. Navig. Control Conf. Exhibit.*, 2006, pp. 63–64.
[17] Y. Liang *et al.*, "Combined vector field approach for planar curved path following with fixed-wing UAVs," in *Proc. Amer. Control Conf.*, Chicago, IL, USA, 2015, pp. 1187–1192.
[18] Y. Liang *et al.*, "Vector field guidance for three-dimensional curved path following with fixed-wing UAVs," in *Proc. Amer. Control Conf.*, Chicago, IL, USA, 2015, pp. 1187–1192.
[19] D. B. Dacic, D. Nesic, and P. V. Kokotovic, "Path-following for nonlinear systems with unstable zero dynamics," *IEEE Trans. Autom. Control*, vol. 52, no. 3, pp. 481–487, Mar. 2007.
[20] A. Morro, A. Sgorbissa, and A. Zaccaria, "Path following for unicycle robots with an arbitrary path curvature," *IEEE Trans. Robot.*, vol. 27, no. 5, pp. 1016–1023, Oct. 2011.
[21] E. Sontag, "Input to state stability: Basic concepts and results," in *Nonlinear and Optimal Control Theory*. Heidelberg, Germany: Springer, 2008, pp. 163–220.
[22] Z.-P. Jiang, A. R. Teel, and L. Praly, "Small-gain theorem for ISS systems and applications," *Math. Control Signals Syst.*, vol. 7, no. 2, pp. 95–120, 1994.
[23] R. Skjetne, "The maneuvering problem," Ph.D. dissertation, Dept. Eng. Cybern., Norwegian Univ. Sci. Technol., Trondheim, Norway, pp. 23–40, 2004.
[24] A. P. Aguiar, J. P. Hespanha, and P. V. Kokotović, "Performance limitations in reference tracking and path following for nonlinear systems," *Automatica*, vol. 44, no. 3, pp. 598–610, 2008.
[25] R. Murray, Z. Li, and S. Sastry, *An Mathematical Introduction to Robotic Manipulation*. Boca Raton, FL, USA: CRC Press, 1994, pp. 100–120.
[26] S. Zhao, X. Wang, D. Zhang, and L. Shen, "Curved path following control for fixed-wing unmanned aerial vehicles with control constraint," *J. Intell. Robot. Syst.*, vol. 89, nos. 1–2, pp. 107–119, 2017.
[27] S. Zhao *et al.*, "Model predictive control based integral line-of-sight curved path following for unmanned aerial vehicle," in *Proc. AIAA Guid. Navig. Control Conf.*, 2017, pp. 1–13.
[28] L. Lapierre and B. Jouvencel, "Robust nonlinear path-following control of an AUV," *IEEE J. Ocean. Eng.*, vol. 33, no. 2, pp. 89–102, Apr. 2008.
[29] A. Brezoescu, T. Espinoza, P. Castillo, and R. Lozano, "Adaptive trajectory following for a fixed-wing UAV in presence of crosswind," *J. Intell. Robot. Syst.*, vol. 69, nos. 1–4, pp. 257–271, 2013.
[30] A. M. Lekkas and T. I. Fossen, "Integral LOS path following for curved paths based on a monotone cubic hermite spline parametrization," *IEEE Trans. Control Syst. Technol.*, vol. 22, no. 6, pp. 2287–2301, Nov. 2014.
[31] I. Kaminer *et al.*, "Path following for small unmanned aerial vehicles using L1 adaptive augmentation of commercial autopilots," *J. Guid. Control Dyn.*, vol. 33, no. 2, pp. 550–564, 2010.

Authors' photographs and biographies not available at the time of publication.